Compact CH_4 sensor system based on a continuous-wave, low power consumption, room temperature interband cascade laser

Lei Dong,[1,2,a)] Chunguang Li,[1] Nancy P. Sanchez,[3] Aleksander K. Gluszek,[1] Robert J. Griffin,[3] and Frank K. Tittel[1]
[1]*Department of Electrical and Computer Engineering, Rice University, Houston, Texas 77005, USA*
[2]*State Key Laboratory of Quantum Optics and Quantum Optics Devices, Institute of Laser Spectroscopy, Shanxi University, Taiyuan 030006, China*
[3]*Department of Civil and Environmental Engineering, Rice University, Houston, Texas 77005, USA*

(Received 8 October 2015; accepted 20 December 2015; published online 5 January 2016)

A tunable diode laser absorption spectroscopy-based methane sensor, employing a dense-pattern multi-pass gas cell and a 3.3 μm, CW, DFB, room temperature interband cascade laser (ICL), is reported. The optical integration based on an advanced folded optical path design and an efficient ICL control system with appropriate electrical power management resulted in a CH_4 sensor with a small footprint ($32 \times 20 \times 17\,cm^3$) and low-power consumption (6 W). Polynomial and least-squares fit algorithms are employed to remove the baseline of the spectral scan and retrieve CH_4 concentrations, respectively. An Allan-Werle deviation analysis shows that the measurement precision can reach 1.4 ppb for a 60 s averaging time. Continuous measurements covering a seven-day period were performed to demonstrate the stability and robustness of the reported CH_4 sensor system. © *2016 AIP Publishing LLC*. [http://dx.doi.org/10.1063/1.4939452]

The ability to monitor methane (CH_4) in urban and rural areas is critical,[1,2] as methane is a key contributor to the greenhouse effect and a safety hazard in several industries, including natural gas storage, transportation, coal mining, and the handling of liquefied methane. Optical methods based on infrared laser spectroscopy are desirable for methane sensing,[3–7] because they do not require pretreatment and accumulation of the concentration of the analyzed sample, unlike, for example, more conventional methods such as mass spectrometry or gas chromatography. In addition, optical methods provide high precision remote sensing capabilities and fast response.

Tunable diode laser absorption spectroscopy (TDLAS) is an increasingly important optical method for trace gas detection.[8–11] In TDLAS either a near or mid-infrared (mid-IR) semiconductor laser source plays an important role. Trace gas species can be detected selectively in real time with sensitivities at ppt concentration levels, using single mode semiconductor lasers, which can be tuned rapidly by varying the drive current. Furthermore, the fundamental v_1 and v_3 CH_4 bands are located at ~7.7 μm and ~3.3 μm, respectively. The absorption line transitions in these two spectral regions are stronger by as much as a factor of ~100 than those of the first overtone band and are therefore better suited for sensitive CH_4 detection. In the wavelength region of ~7.7 μm, high detection sensitivity for the methane measurements using quantum cascade lasers (QCLs) have been reported.[12,13] However, single mode, room temperature laser sources emitting continuous-wave (CW) in the 3–4 μm range with reasonable output and low electrical power consumption became only recently commercially available. Commercially obtainable QCLs are limited to wavelengths above 3.7 μm.[14] This led to a wavelength range referred to as the "mid-infrared gap" in TDLAS based on spectroscopic trace gas sensing. In 2009, a gallium antimonide (GaSb)-based interband cascade laser (ICL) design initiated a new pathway for mid-IR sensing.[15–17] Laser diodes based on such a design provide CW radiation between 3.0 μm and 6.0 μm at room temperature. ICLs, like QCLs, are compact and an intrinsic distributed feedback (DFB) structure permits CW tuning with spectral linewidths of <10 MHz.

The other key component in TDLAS is the multi-pass gas cell (MPC), which provides a sufficiently long absorption path length for trace gas sensing, because the measurement sensitivity is improved by increasing the effective optical path length.[18] However, conventional White and Herriott gas cells[19,20] with absorption path lengths on the order of 10 m have typical physical lengths of ~30 cm and volumes of 250 ml for a Herriott cell and 2 l for a White cell, which is an unsatisfactory match for a compact sensor system. This mismatch in sizes was addressed by Sentinel Photonics/Aeris Technologies through the design and development of an ultra-compact MPC consisting of two inexpensive standard concave spherical mirrors using a dense spot pattern, which is more complex than the typical traditional circular or elliptical beam patterns.[21,22] Such an MPC design offers a 54.6-m optical path length in a physical size of $17 \times 6.5 \times 5.5\,cm^3$ with a 220-ml sampling volume and thereby obtains a sensor platform that is more than 10 times smaller than conventional designs with equivalent sensitivity. In this manuscript, we report on the development of a compact, low power consumption CH_4 sensor system using the combination of two recent techniques: a compact ICL and a small MPC.

A 3D CAD model of the optical core of the methane sensor discussed is shown in Fig. 1(a). Its schematic and final configuration are shown in Fig. 1(b). A Nanoplus GmbH, CW, DFB ICL mounted in a TO66 header emitting single-mode

a)Electronic mail: donglei@sxu.edu.cn

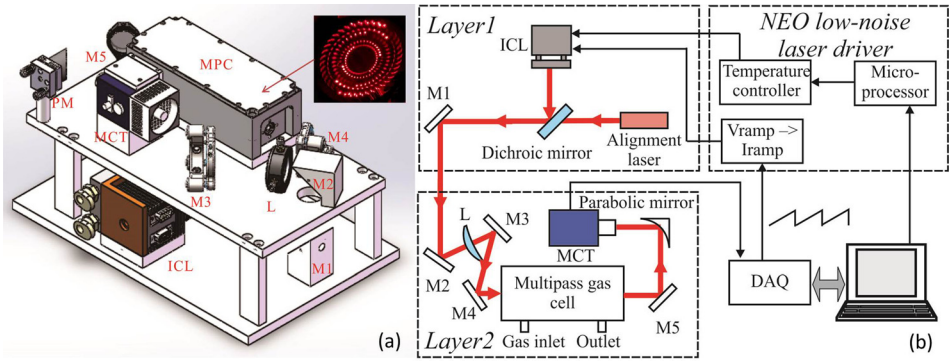

FIG. 1. (a) CAD image of the methane sensor core with dimensions of length (32 cm), width (20 cm), and height (17 cm). Inserted image: dense spot pattern of the ultra-compact multi-pass gas cell. (b) Schematic of a compact, low power methane sensor. ICL: interband cascade laser; L: lens; M: plane mirror; MCT: mercury-cadmium-telluride detector; MPC: multi-pass gas cell; PM: parabolic mirror.

radiation at a center wavelength of 3291 nm was employed as the light source. The TO66 header was enclosed in a $5 \times 5 \times 5\,\text{cm}^3$ cubic heat sink with a thermoelectric cooler (TEC). The ICL output power is 1.5 mW at an operating temperature of 30 °C, requiring a drive current of 42 mA. The measured current and temperature tuning coefficients of the ICL are $-0.232\,\text{cm}^{-1}$/mA and $-0.240\,\text{cm}^{-1}/°\text{C}$, respectively.

A three dimensional folded optical path design was adopted in order to minimize the sensor size. The CH_4 sensor system design consists of two layers, as shown in Fig. 1. The ICL, an alignment laser, and a dichroic mirror were mounted on the bottom layer (*Layer* 1). An alignment diode laser emitting visible radiation at 630 nm was used as a guide beam for the invisible mid-IR ICL beam. The two laser beams, visible and mid-IR, were combined by means of a dichroic mirror (ISO optics, model BSP-DI-25-3). A 45°-angle plane mirror (M1) with respect to the horizontal plane directed the combined beams from the bottom layer (*Layer 1*) to the top layer (*Layer 2*). A second plane mirror (M2) converted the combined laser beams from the vertical to the horizontal direction. The top layer (*Layer 2*) includes the MPC, the mid-IR detector, and five auxiliary optical components. The co-propagating beams were coupled into the MPC using a mode matching lens of 200-mm focal length (L). Two plane mirrors (M3 and M4) fold the necessary optical path as the focal point of the lens must be positioned at the MPC entry aperture. The enclosure of the MPC was made of super invar with a typical mean coefficient of thermal expansion of $10^{-6}/°\text{C}$. The dense spot pattern of the MPC obtained with the red alignment diode laser is shown in the insert in Fig. 1(a). An effective optical path length of 54.6 m was obtained after 435 beam passes in the MPC. The exiting, collimated ICL beam from the MPC was subsequently focused onto a TEC, mercury-cadmium-telluride (MCT) detector (Vigo, PVI-4TE-4) using first a plane mirror (M5) and then a 35-mm focal length parabolic mirror. Dowel pins made of stainless steel were used as supports between the top and bottom layers to ensure stability of the two layers of the sensor system assembly. Our design of an optical core consisting of two layers possessed the same thermal stability with our previous single layer system.[22]

Selection of the optimum target absorption line is a key factor that ultimately affects the size, cost, and complexity of the CH_4 sensor system. A single methane line, ν_3R(1), which is located at $3038.5\,\text{cm}^{-1}$ and is free from the interference of other atmospheric gases was selected as the target line to determine methane concentration levels. This methane absorption line has a line intensity of 8.958×10^{-20} cm/molecule. Furthermore, this selected line allows operation of the sensor at atmospheric pressure thereby avoiding the use of a vacuum pump.

A compact, low-noise laser driver developed by NEO Monitors, SA, Norway, was employed to operate the ICL as shown in Fig. 1(b). The laser driver board has a size of 10 cm × 8 cm with a low noise current characteristic of $\leq 1\,\text{nA}/\sqrt{\text{Hz}}$ and an on-board TEC driver (±3 A, 15 V). The TEC driver was programmed to control the ICL temperature to 30 °C. Potential use of the methane sensor for field studies involving mobile-mode sampling requires effective and reliable electrical power management of the different components in the sensor system. The maximum TEC current and voltage determines the TEC power consumption of 5.3 W. A 12-V power supply was used because this voltage is compatible with car batteries. With a maximum laser current of 50 mA, the ICL requires 0.6-W power. Hence, the total power consumption for the sensor system is ~6 W. A laptop equipped with a NI DAQ card (NI 6062E) was used to generate the 500 Hz sawtooth wave with an offset of 2.1 V and a peak-peak amplitude of 0.4 V, which was sent to the ramp input of the ICL driver, resulting in an ICL current scan from 38.3 mA to 46.1 mA. This current range corresponds to a wavelength range from $3038.04\,\text{cm}^{-1}$ to $3039.03\,\text{cm}^{-1}$. Furthermore, the laptop synchronously acquires the spectral data from the MTC detector with a sampling rate of 250 kS/s.

A typical methane spectrum of laboratory air is depicted in Fig. 2 together with a transmission signal from a 2.54-cm

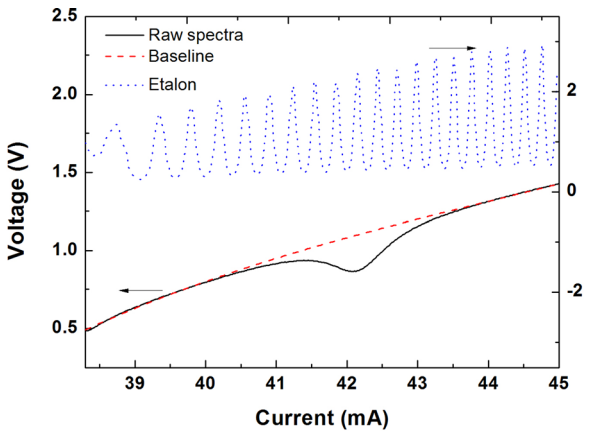

FIG. 2. Interference-free absorption line of CH_4 at $3038.5\,\text{cm}^{-1}$ obtained from laboratory air at atmospheric pressure together with a fitted baseline and a transmission signal from a Germanium etalon.

long Germanium etalon with a free spectral range of 1.44 GHz. The acquired methane spectrum was processed using a four-step algorithm. In the first step, 150 methane spectra were averaged, and the absorption peak is removed from the averaged spectra. In the second step, the baseline of the spectral scan was fitted and eliminated using a fifth order polynomial as shown in Fig. 2 (dashed line). In the third step, the resulting spectrum is linearized using the quadratic polynomial obtained from the Ge etalon fringe spacing. Finally, a Lorentzian line shape was fitted to the absorption peak using a Levenberg-Marquardt least-squares fit procedure.[23] A three-threaded program compiled by Labview executed the ramp signal output, the signal acquisition, and the digital signal processing in parallel via the NI DAQ card. Because the concentration retrieval algorithm is based on the Beer-Lambert law, it is possible to provide an absolute quantitative assessment without any calibration. The electronic system bandwidth of 300 kHz is determined by the preamplifier of the MCT detector. Spectral averaging resulted in an effective bandwidth of 2 kHz.[24] The resulting output rate of the methane sensor is 1 Hz with a 30% duty cycle (data acquisition time of a 300 ms/measurement time 1000 ms).

To assess the long-term stability of the methane sensor, an Allan-Werle deviation analysis was implemented based on continuous measurements of a certified 2 ppm CH_4:N_2 mixture (Coastal specialty gas, accuracy ±5%) in time periods lasting ~1.5 h, as shown in Fig. 3. This indicates that the 1-s measurement precision is $\sigma = 10.53$ ppb. The Allan-Werle plot shows an optimum integration time of ~60 s, corresponding to a precision of ~1.43 ppb. The dashed line, proportional to $1/\sqrt{t}$, depicts the theoretically expected behavior of a system within the white noise dominated region. The Allan-Werle deviation of the reported sensor follows the $1/\sqrt{t}$ dependence for >60 s, after which time system drifts start to dominate. Based on the absorption line strength, a gas pressure of 760 Torr, an optical path length of 54.6 -m, and an effective bandwidth of 2 kHz, a normalized noise equivalent absorption coefficient (NNEA) of 1.34×10^{-7} cm$^{-1}/\sqrt{\text{Hz}}$ was achieved. The NNEA is one order of magnitude higher than the NNEA of 2.5×10^{-8} cm$^{-1}/\sqrt{\text{Hz}}$ obtained for the methane detection at 7.7 μm.[12] The main reason for this is the NI DAQ card used in the system, which limits the maximum output frequency of the ramp signal for scanning the ICL wavelength to 500 Hz.

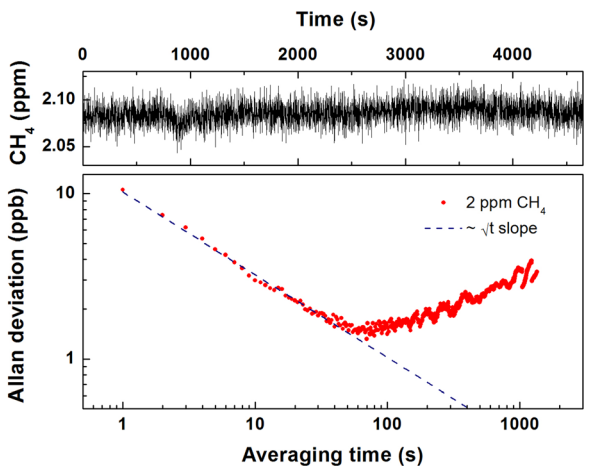

FIG. 3. Allan-Werle deviation plot acquired from measurements using a certified 2 ppm CH_4 cylinder with a 1 Hz sampling rate.

The CH_4 sensor system operated at 1 s measurement time and was located in the Space Science and Technology building on the Rice University campus. A small pump was used to sample air from outdoors. Due to the pressure gradient, the inside pressure of the MPC is 700 Torr. The methane mixing ratios measured for seven days of continuous monitoring (May 1 to May 8, 2015) are shown in Fig. 4(a). The average methane concentration was 1.96 ± 0.1 ppm, with maximum and minimum concentrations of 2.7 and 1.8 ppm, respectively. According to Fig. 4(a), slightly higher methane levels were observed during the weekend (May 2 and 3, 2015) relative to weekdays (May 4-May 8, 2015), though longer sampling would be required to determine if weekend-weekday differences are statistically significant. The diurnal profile of methane concentration (Fig. 4(b)) shows an increase in methane concentration during the early morning, with a subsequent gradual decrease after ~8:00 CDT to its typical background level of ~1.87 ppm. The early morning peak and the diurnal trends observed in methane mixing ratios during the sampling period are in agreement with previous research.[1]

In conclusion, a TDLAS based CH_4 sensor system, employing an MPC with a >50 m optical path length and a CW, DFB ICL capable of room temperature operation was developed. A three dimensional folded optical path design

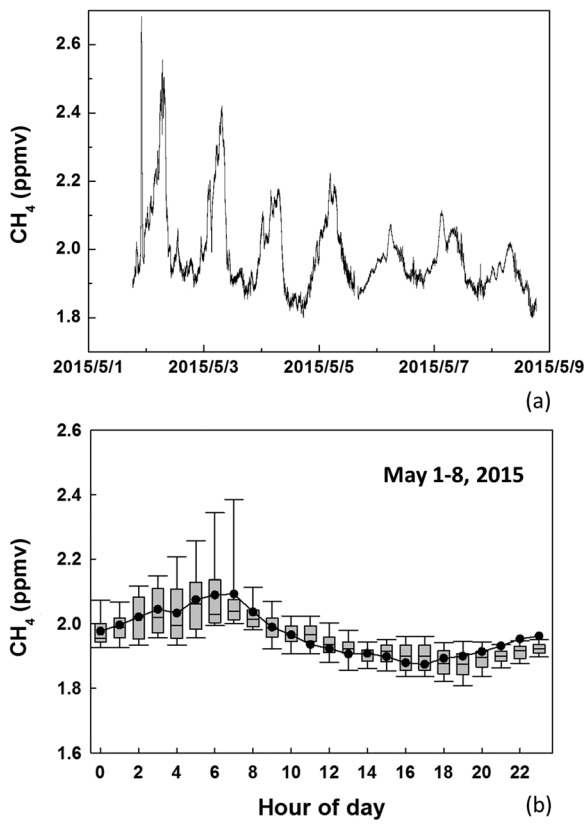

FIG. 4. (a) CH_4 concentrations measured over a 7 day period on the Rice University campus. (b) Diurnal variations of CH_4 mixing ratios. Bottom whisker, bottom box line, top box line, and top whisker indicate the 5th, 25th, 75th, and 95th percentiles, respectively. Line inside the boxes and continuous solid line represent the hourly median and mean of the data, respectively.

and reduced electrical power management resulted in a sensor system with a small footprint ($32 \times 20 \times 17\,cm^3$) and low electrical power consumption (6 W). Our results show that the measurement precision of the sensor is 10.5 ppb for a 1-s averaging time and can be improved to 1.4 ppb with a 60-s averaging time. Deployment of the sensor system in a vehicle and mobile-mode operation tests to evaluate its performance for atmospheric methane monitoring will be conducted in the future.

Frank Tittel acknowledges support by the Robert Welch Foundation (Grant C-0586). Frank Tittel, Nancy Sanchez, and Robert Griffin acknowledge support by the National Science Foundation (NSF) ERC MIRTHE award. Lei Dong acknowledges support by National Natural Science Foundation of China (Grant Nos. 61575113 and 61275213).

[1]I. Bamberger, J. Stieger, N. Buchmann, and W. Eugster, Environ. Pollut. **190**, 65 (2014).
[2]F. A. Smith, S. Elliott, D. R. Blake, and F. S. Rowland, Environ. Sci. Policy **5**, 449 (2002).
[3]D. G. Lancaster, R. Weidner, D. Richter, F. K. Tittel, and J. Limpert, Opt. Commun. **175**, 461 (2000).
[4]D. G. Lancaster and J. M. Dawes, Appl. Opt. **35**, 4041 (1996).
[5]C. Fischer and M. W. Sigrist, Appl. Phys. B **75**, 305 (2002).
[6]D. Richter, D. G. Lancaster, R. F. Curl, W. Neu, and F. K. Tittel, Appl. Phys. B **67**, 347 (1998).
[7]K. P. Petrov, S. Waltman, E. J. Dlugokencky, M. Arbore, M. M. Fejer, F. K. Tittel, and L. W. Hollberg, Appl. Phys. B **64**, 567 (1997).
[8]H. I. Schiff, G. I. Mackay, and J. Bechara, Res. Chem. Intermed. **20**, 525 (1994).
[9]K. Krzempek, R. Lewicki, L. Nähle, M. Fischer, J. Koeth, S. Belahsene, Y. Rouillard, L. Worschech, and F. K. Tittel, Appl. Phys. B **106**, 251 (2012).
[10]M. Köhring, S. Huang, M. Jahjah, W. Jiang, W. Ren, U. Willer, C. Caneba, L. Yang, D. Nagrath, W. Schade, and F. K. Tittel, Appl. Phys. B **117**, 445 (2014).
[11]W. Ren, L. Luo, and F. K. Tittel, Sens. Actuators, B **221**, 1062 (2015).
[12]W. Ren, W. Jiang, and F. K. Tittel, Appl. Phys. B **117**, 245 (2014).
[13]P. C. Castillo, I. Sydoryk, B. Gross, and F. Moshary, Proc. SPIE **8718**, 87180J (2013).
[14]S. Suchalkin, G. Belenky, and M. A. Belkin, IEEE J. Sel. Top. Quant. Elec. **21**, 1200509 (2015).
[15]L. Nähle, L. Hildebrandt, M. Kamp, and S. Höfling, Laser Focus World **49**, 70 (2013), http://www.laserfocusworld.com/articles/print/volume-49/issue-05/features/interband-cascade-lasers–icls-open-opportunities-for-mid-ir-sen.html.
[16]I. Vurgaftman, W. W. Bewley, C. L. Canedy, S. K. Chul, K. Mijin, C. D. Merritt, J. Abell, and J. R. Meyer, IEEE J. Sel. Top. Quant. **19**, 1200210 (2013).
[17]A. Bauer, F. Langer, M. Dallner, M. Kamp, M. Motyka, G. Sek, K. Ryczko, J. Misiewicz, S. Höfling, and A. Forchel, Appl. Phys. Lett. **95**, 251103 (2009).
[18]Y. Cao, N. Sanchez, W. Jiang, R. J. Griffin, F. Xie, L. C. Hughes, C. Zah, and F. K. Tittel, Opt. Exp. **23**, 2121 (2015).
[19]D. R. Herriot and H. J. Schulte, Appl. Opt. **4**, 883 (1965).
[20]J. U. White, J. Opt. Soc. Am. **32**, 285 (1942).
[21]G. Overton, Laser Focus World **49**, 17 (2013), http://www.laserfocusworld.com/articles/print/volume-49/issue-08/world-news/metrology-new-multipass-gas-cells-beat-conventional-designs.html.
[22]L. Dong, Y. Yu, C. Li, S. So, and F. K. Tittel, Opt. Express **23**, 19821 (2015).
[23]D. Rehle, D. Leleux, M. Erdelyi, F. Tittel, M. Fraser, and S. Friedfeld, Appl. Phys. B **72**, 947 (2001).
[24]P. Werle, R. Mücke, and F. Slemr, Appl. Phys. B **57**, 131 (1993).